


YANNIC EGE, CHRISTIAN FOTH, DANIEL BAUM<sup>1</sup>,  
CHRISTIAN S. WIRKNER, STEFAN RICHTER

**Making spherical-harmonics-based  
Geometric Morphometrics (SPHARM)  
approachable for 3D images containing  
large cavity openings using Ambient  
Occlusion - a study using hermit crab  
claw shape variability**

---

<sup>1</sup>  0000-0003-1550-7245

Zuse Institute Berlin  
Takustr. 7  
14195 Berlin  
Germany

Telephone: +49 30-84185-0  
Telefax: +49 30-84185-125

E-mail: [bibliothek@zib.de](mailto:bibliothek@zib.de)  
URL: <http://www.zib.de>

ZIB-Report (Print) ISSN 1438-0064  
ZIB-Report (Internet) ISSN 2192-7782

# **Making spherical-harmonics-based Geometric Morphometrics (SPHARM) approachable for 3D images containing large cavity openings using Ambient Occlusion - a study using hermit crab claw shape variability**

**Yannic Ege<sup>1</sup>, Christian Foth<sup>2</sup>, Daniel Baum<sup>3</sup>, Christian S. Wirkner<sup>1</sup>, Stefan Richter<sup>1</sup>**

<sup>1</sup>Allgemeine & Spezielle Zoologie, Institut für Biowissenschaften, Universität Rostock, Rostock, Germany

<sup>2</sup>Department of Geosciences, Université de Fribourg, Fribourg, Switzerland

<sup>3</sup>ZIB - Zuse Institute Berlin, Berlin, Germany

Correspondence : Yannic Ege, Allgemeine & Spezielle Zoologie, Institut für Biowissenschaften, Universität Rostock, Universitätsplatz 2, 18055 Rostock, Germany. E : yannic.ege@uni-rostock.de

## **Abstract**

An advantageous property of mesh-based geometric morphometrics (GM) towards landmark-based approaches, is the possibility of precisely examining highly irregular shapes and highly topographic surfaces. In case of spherical-harmonics-based GM the main requirement is a completely closed mesh surface, which often is not given, especially when dealing with natural objects. Here we present a methodological workflow to prepare 3D segmentations containing large cavity openings for the conduction of spherical-harmonics-based GM. This will be exemplified with a case study on claws of hermit crabs (Paguroidea, Decapoda, Crustacea), whereby joint openings – between manus and “movable finger” – typify the large-cavity-opening problem. We found a methodology including an ambient-occlusion-based segmentation algorithm leading to results precise and suitable to study the inter- and intraspecific differences in shape of hermit crab claws. Statistical analyses showed a significant separation between all examined diogenid and pagurid claws, whereas the separation between all left and right claws did not show significance. Additionally, the procedure offers other benefits. It is easy to reproduce and creates sparse variance in the data, closures integrate smoothly into the total structures and the algorithm saves a significant amount of time.

**Key words:** geometric morphometrics, spherical harmonics, ambient occlusion, shape comparison, hermit crabs

## **Introduction**

### **Paguroidea**

Hermit crabs (Paguroidea, numbering over 1100 species) represent a fascinating and likewise one of the most successful taxa within decapod crustaceans (Decapoda). The groups' most conspicuous anatomical feature is the soft-shelled pleon, which is hidden within a snail shell in most of the species. Phylogenetically, king crabs (Lithodoidea) and the terrestrial Coenobitidae, e.g. the coconut crab (*Birgus latro*), also belong to the hermit crabs. Not less interesting are the first walking legs, which are formed as chelipeds and can reach astonishing sizes in relation to body length. There are hermit crabs with a prominent right (Paguridae, Lithodoidea) respectively a prominent left (Diogenidae, Coenobitidae) claw (chela), however some species display no discrepancy in claw size (Pylochelidae,

some Diogenidae). Various tasks (e.g. biological roles) are being carried out by these claws, most common are food manipulation, use as weapons to fight potential predators or other threats as well as shell closure. Depending on the taxon, closure of the shell can be ensured by the right, the left or both chelipeds. For food consumption, the claws overall shape is apparently less relevant than the cutting edge between the immovable and movable finger (propodus and dactylus, respectively). Characteristics of the dentition of the cutting edges apparently resemble different types of pliers regarding their function (Schäfer 1954). Since handedness within paguroidean taxa is genetically fixed and therefore serves as phylogenetic feature, the comparison of claw shape is very meaningful, especially between left- and right-handed taxa.

### **Geometric morphometrics**

Modern geometric morphometrics provide meaningful methods to identify and quantify variations in shape of structures (Mitteroecker & Gunz 2009, Schultz et al. 2016) and thereby a first aspect in the detailed examination of a form-function-complex (e.g. crab claws). In contrast to classic morphometrics, the performance of a superimposition, the Procrustes Fit, normalizes respectively standardizes the size, position and the orientation of structures (morphemes *sensu* Richter & Wirkner 2014). This is usually done with the help of *Generalized Procrustes Analyses* (GPA) (Gower 1975) and allows the performance of a purely shape-dependent statistical analysis (Hammer & Harper 2006, Zelditch et al. 2012). Prior to the analysis, points have to be chosen, which are homologous and recognizable in all structures to be examined, the so-called landmarks (Bookstein 1991, 1997). Landmark-based approaches are successful for many cases in GM but are restricted to one decisive factor: the replicability of points in all investigated structures. For objects missing such points as spherical or rounded structures, e.g. in claws, this becomes a problem.

To capture the morphologic features of spherical and rounded structures, semi-landmarks can be used, which are a set of points on homologous curves or surfaces with positions along the object that cannot be exactly determined by true landmarks (Mitteroecker & Gunz 2009). By applying the sliding landmark algorithm (Bookstein 1997, Gunz et al. 2005), positions of semi-landmarks can be estimated along the curve and thus are used to depict these features. Homologous curves can also be defined using consistent distances between semi-landmarks throughout all objects in question. But in terms of defining highly irregular shapes or highly topographic surfaces, even semi-landmarks quickly reach their limitations.

Recent methods in shape analysis like the *Semi-Automated Landmarking Procedure* (Felice & Goswami 2017) and *Generalized Procrustes Surface Analysis* (Pomidor et al. 2016) tackle this difficulty and are more precise in capturing curvatures and surfaces. Also, approaches based on spherical harmonics (SPHARM), which represent an extension of Fourier analyses, enable the possibility of an accurate comparison of overall shape, including structures that are highly irregular in shape and size and contain only few definable and morphological suitable points where landmarks can be set. Taking the whole object into account, the previously mentioned methods provide a more objective approach of shape comparison, which is in our opinion an ultimate goal in comparative morphology. In this study we used the open source software *SPHARM* v. 1.4 (<http://www.enallagma.com/SPHARM.php>; Shen & Makedon 2006, Shen et al. 2009). As the name suggests, the software is based on SPHARM and generates 3D mathematical models of object surfaces (Brechtbühler et al. 1995). The software has

helped to understand the coevolution of reproductive organs in damselflies on a morphological basis (McPeck et al. 2009, 2011) and was also successfully used to investigate shape patterns of frontal sinuses in Carnivora (Curtis & van Valkenburgh 2014). More recently, it was applied to exploring the relationship between habitat preferences and the middle ear shape of turtles (Foth et al. 2019).

The fact that SPHARM can only be used on models with completely closed surfaces results in the question of how to deal with structures exhibiting large openings, like single segments of arthropods. One can argue that the openings do not belong to the studied feature itself and should not be considered for shape comparison at all but this is only partly true. The margin of such an opening does have a certain shape and this shape also contributes to the shape of the entire feature. This means the inclusion of openings to the overall shape of studied objects is necessary and the problem that SPHARM-based applications only work on models with completely closed surfaces has to be faced.

### **Ambient occlusion**

There are some software applications, which can be used to identify and close small holes in generated mesh surfaces (e.g. *MeshLab*, *Geomagic Studio* and *Deep Exploration*) but when it comes to holes which have to be closed before even generating a surface for SPHARM-based analyses, capabilities are quickly exhausted. For this purpose, we applied an ambient-occlusion-based (AO) segmentation algorithm using *Amira* (Baum & Titschack 2016) to our segmented datasets. Based on a separation of the data into foreground (object) and background (rest), the AO algorithm computes an approximation for how much each point of the background would be occluded from ambient light, hence the name of the algorithm. An advantageous property of AO is that it generates smooth scalar fields and, thus, subsequent segmentations based on those scalar fields result in smooth boundaries at pores and cavity openings. This is a very desirable property, particularly when dealing with natural objects. The usage of this algorithm comes with three main advantages: (1) it is a mathematically-based closing procedure that is easy to reproduce, generates less variance in the data than hand-made closures and is thus well-suited to represent the shape of closed openings; (2) it mostly creates closures that integrate smoothly into the total structures; and (3) it saves a significant amount of time as opposed to creating handmade closures.

A requirement for the algorithm is the classification of input data into *background* and *foreground*, that is, a binary segmentation, which is often generated previous to computing a surface representation anyway. Openings and holes to be extracted, as well as the structures outside are part of the background, whereas the structures themselves are categorized as foreground. In order to determine the amount of ambient light that can reach a certain point in the background, a large number of directions is considered given by the points that are uniformly sampled on a full sphere. In contrast to the typical usage of AO for shading surfaces in computer graphics, which only considers a hemisphere close to the surface, the herein used algorithm considers the directions on a full sphere at each point of the background. The algorithm works by casting rays from each point (voxel) of the background into all directions given by uniformly sampled points on the sphere. For each ray, it is determined whether or not the ray hits a foreground voxel. The number of rays that hit the foreground divided by the overall number of rays gives the AO value for each background voxel. Those values are output as a scalar field, the AO field.

## Claw shape comparison

We exemplify the topic with a preliminary study on shape comparison of claws in hermit crabs. The articulation socket between propodus (forming the manus as well as the pollex, the fixed finger) and dactylus (the movable finger) are depicted as hole as well as the articulation socket between propodus and the next more proximal element, the carpus. We applied a methodology including an ambient-occlusion-based segmentation algorithm to test whether the algorithm results in precise and suitable shape representations detailed enough to study the inter- and intraspecific differences in shape of hermit crab claws. Obviously, for a comparison one of the chelae needs to be mirrored.

## Materials and methods

### Studied Species

In total we studied 18 specimens of paguroid species, which are summarized in Table 1. Except for one, all specimens were collected in 2017 along the Istrian coastline respectively the Kvarner Gulf, Croatia. All specimens were stored in 70% EtOH.

**Table 1.** Studied paguroid species. HRV - Croatia, SWE - Sweden.

| Species  | Taxon      | sex    | locality            | date       |
|--|------------|--------|---------------------|------------|
| <i>Clibanarius erythropus</i><br>(LATREILLE, 1818) | Diogenidae | male   | Krk (HRV)           | 25.09.2017 |
|  |            | female | Krk (HRV)           | 25.09.2017 |
|  |            | female | St. Baška (HRV)     | 26.09.2017 |
| <i>Diogenes pugilator</i><br>(ROUX, 1829)          | Diogenidae | male   | Krk (HRV)           | 26.09.2017 |
|  |            | female | Krk (HRV)           | 26.09.2017 |
|  |            | female | Krk (HRV)           | 26.09.2017 |
| <i>Paguristes eremita</i><br>(LINNAEUS, 1767)      | Diogenidae | male   | Krk (HRV)           | 02.06.2017 |
|  |            | male   | Krk (HRV)           | 02.06.2017 |
|  |            | male   | Pula (HRV)          | 29.09.2017 |
| <i>Paguristes streasensis</i><br>(PASTORE, 1984)   | Diogenidae | female | Pula (HRV)          | 31.08.2017 |
|  |            | male   | Pula (HRV)          | 31.08.2017 |
|  |            | male   | Pula (HRV)          | 29.09.2017 |
| <i>Pagurus anachoretus</i><br>(RISSO, 1827)        | Paguridae  | male   | St. Baška (HRV)     | 26.09.2017 |
|  |            | male   | St. Baška (HRV)     | 26.09.2017 |
|  |            | male   | St. Baška (HRV)     | 26.09.2017 |
| <i>Pagurus cuanensis</i><br>(BELL, 1846)           | Paguridae  | male   | Plavnik (HRV)       | 08.07.2017 |
|  |            | male   | St. Baška (HRV)     | 26.09.2017 |
|  |            | female | Gullmarsfjord (SWE) | 15.08.2007 |

### Fixation and Dehydration

Preparing for microCT scanning, an ascending alcohol series for dehydration using 70, 80, 90, 96 and 99.8 percent EtOH, was conducted with the claws of the listed specimens. Afterwards, the claws were supercritical dried (Leica EM CPD300) to enhance contrast in CT images. We spared further contrasting methods, since the contrast of dried, calcified cuticles is sufficient for shape analyses using microCT.

## Micro Computer Tomography

Dried chelipeds were mounted with hot glue on specimen holders. X-ray imaging was performed with a ZEISS Xradia 410 Versa (Carl Zeiss Xray Microscopy Inc., Pleasanton, USA) at 50 - 80 KV and 8 W (0.4 scintillator-objective lens unit, 5 - 12  $\mu\text{m}$  pixel size).

## Work Flow

Here, we describe the complete work flow used to generate SPHARM-based surface models of the compiled microCT scans, including the conduction of PCA. Programs used were *Amira*, *MeshLab* and *SPHARM*.

### 3D Surface Reconstruction and AO segmentation - *Amira*

3D reconstruction was performed using image stacks of virtual sections obtained by microCT. All reconstructions were created using the software *Amira* (FEI Visualization Sciences Group, Zuse Institute Berlin, 6.4.0). After saving segmentations of claw podomeres (propodus and dactylus) separately as *Amira* label files (Figure 1b), the AO-based segmentation algorithm was applied to each segmentation (the *XImagePAQ* extension of the latest *Amira* version (2019) includes the proposed AO segmentation algorithm as a standard application). For best results in this case, the AO value of the segmentation algorithm was set to 0.7 for all structures (Figure 1d). Since transition lines between the computed closures and the segmentations were still visible, further smoothing was achieved using the smooth function in *Amira* (x-y, x-z and y-z plane). Afterwards the merged totals of closures and segmentations were used to calculate surface models (rendering) of the podomeres by using the module *Generate Surface*. A first reduction of vertices and faces was done using the *Simplification Editor* application in *Amira*. Thereby surfaces were downscaled by one third. Then the *Remesh Surface* and the *Smooth Surface* modules were applied. For further data processing, the generated surfaces were exported as PLY data files using *MeshLab* v. 1.3.4beta (Visual Computing Lab, ISTI, CNR).

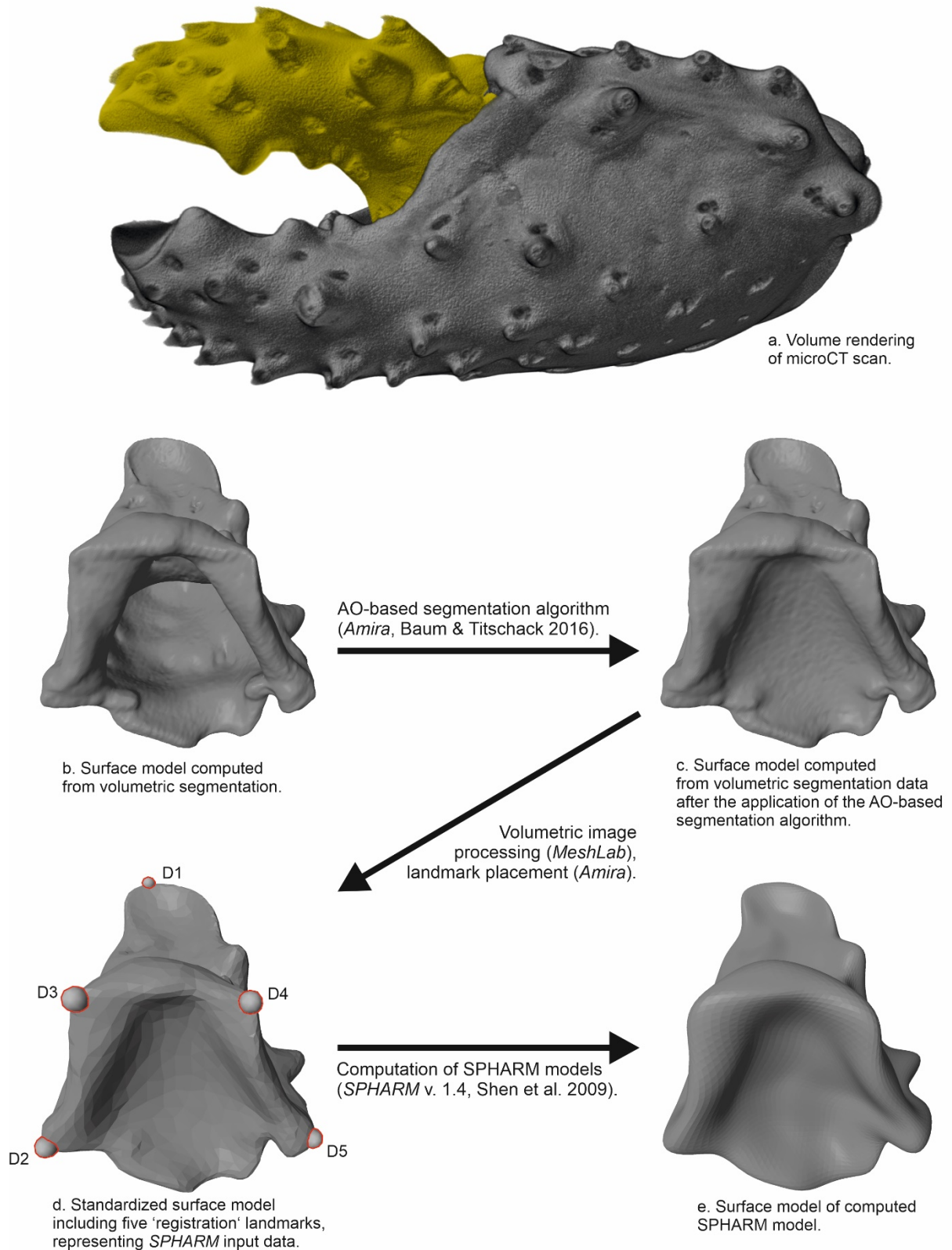


**Figure 1:** (a) Depiction of the left claw of *Clibanarius erythropus* (dactylus highlighted in yellow) in lateral view. Further processing steps are exemplified on the left dactylus of *C. erythropus* (rotated through 180° along the long axis and shown in distal view). (b) Volumetric segmentation before and after (c) the application of the AO-based segmentation algorithm. Figure (d) shows the standardized surface model including the set of orientation landmarks and (e) the finished SPHARM model. D1 - distal dactylus ending, D2 - median joint surface to propodus, D3 - median boundary of closure apodem, D4 - lateral boundary of closure apodem, D5 - lateral joint surface to propodus.



### 3D Mesh Processing - *MeshLab*

Most mesh processing steps were conducted using *MeshLab* (Cignoni et al. 2008) and are listed in chronological order in the following protocol. The program contains features for detecting and correcting errors in mesh geometry that can occur. All used processing steps can be found in the tab *Filters*. Furthermore, we used the standard settings of processing steps where parameters could be adjusted. Again, following these steps, the corrected and processed surfaces were exported as PLY data files.

1. Option *Cleaning and Repairing*  
Processing steps *Remove Duplicate Faces*, *Remove Duplicate Vertices* and *Remove Unreferenced Vertices*.
2. Option *Remeshing, Simplification and Reconstruction*  
Processing steps *Close Holes*, *Surface Reconstruction: Poisson* and *Quadric Edge Collapse Decimation* (number of faces / vertices was set to 5000 / 2502 for dactyli and 10000 / 5002 for propodi).
3. Option *Smoothing, Fairing and Deformation*  
Processing step *Taubin Smooth*.
4. Option *Normals, Curvatures and Orientation*  
Processing steps *Transform: Flip and/or swap axis* and *Invert Faces Orientation* (both steps were only conducted with the right podomeres, since they were necessary for mirroring).

### Landmarks - *Amira*

A set of five orientation landmarks were applied for scaling, rotating, and aligning specimens before SPHARM analyses could be conducted. The landmarks were set on the standardized surface models in *Amira* (Figure 1d), and were exported as landmarkAscii files.

### Geometric Morphometrics - *SPHARM*

Prior to the conduction of SPHARM analyses with the 3D surface models, they had to be converted into *Matlab* (M) data files, since *SPHARM* v. 1.4 is written in *Matlab* (The MathWorks, <https://de.mathworks.com/products/matlab.html>). Used options were *Make Models From Input Files*, *Make Surfaces From SPHARM Models* and *Principal Components Analysis*. Again, standard settings of the tasks were used.

1. Option *Make Models From Input Files*  
Surface and landmark data were loaded in *SPHARM* v. 1.4. In the first processing step (*Resize Objects & Landmarks*), the 'Resize' and 'Centroid' options were activated to superimpose all surface models on the basis of the orientation landmarks using GPA. Calculated centroid sizes (CS) were saved as TXT file.  
In the second processing step (*Make Template*), a spherical parameterization was conducted to determine a reference dataset. In our case the logarithm of the median of all CS was calculated and the M data file with the log(CS) closest to the median was chosen as template.

For the third processing step (*Make SPHARM Models*), the template and the corresponding M data files had to be selected. After the performance of this step, there were three output data files per uploaded M data file. The reg\_MAT data files contained the corresponding SPHARM model coefficients for further analyses.

2. Option *Make Surfaces From SPHARM Models*

This option can be seen as a last check of input data before executing the PCA. On the basis of the reg\_MAT data files, surfaces were compiled (Figure 1e), which could then be reviewed for surface artifacts and falsely set landmarks using *Amira* or similar programs.

3. Option *Principal Components Analysis*

In this option, the previously checked reg\_MAT data files (36 for dactyli and 36 for propodi) were uploaded. Afterwards the conduction of PCAs took place (one PCA for each podomere data set). Output data consisted of 35 PCs. Eigenvalue models of the PCs including the consensus shapes were calculated as surfaces (Figure 2). Numerical summaries of PCAs (total variance, eigenvalue of PCs, explained variance of PCs and PC results) were compiled as DTA data files.

## **Multivariate statistics**

PCs with significant shape variation were calculated with the help of the broken stick method (Jackson 1993) performed in *PAST* v3.18 (Hammer et al. 2001). To test whether right and left podomers of representatives of Diogenidae and Paguridae species overlap with each other or are significantly separated from each other in morphospace, multivariate analyses of variance (MANOVA) and nonparametric multivariate analyses of variance (npMANOVA) were also performed in *PAST*. Furthermore, classifications into diogenid left, diogenid right, pagurid left and pagurid right dactyli and propodi were also tested with MANOVA, npMANOVA and a canonical variate analysis (CVA). If the p values of each test were below 0.05, a significant separation between two groups within the morphospace was given.

## Results

### Dactyli shape variation

The first four PCs define significant shape variation, explaining 80.1% of total shape variation (PC1: 31.3%; PC2: 22.3%; PC3: 16.3% and PC4: 10.2%).

Regarding PC1, negative values (Figure 2b) include shortened dactyli with a dominant appearance, regarding the bigger extend, the distinct cutting edge and the enlarged insertion point. Positive values of this component account for an elongated dactylus with a small extend compared to the consensus shape (Figure 2a). Also, the cutting edge is more rounded and therefore appears less dominant.

Shape changes associated with negative values of PC2 (Figure 2d) show dorsally flattened dactyli with a ventromedially twisted tip. Also, the cutting edge is proximally elongated. The dorsal part of the insertion point is posteriorly tilted. Positive values of PC2 (Figure 2e) represent longitudinally bent dactyli with a waved cutting edge and insertion points standing in a 90° angle to the long axis.

Negative values of the third PC (Figure 2f) account for dactyli exhibiting a strong bending along the dorsal long axis, as well as a centered, broad cutting edge. They also exhibit a joint opening that is anteriorly tilted in the ventral part. In contrast, positive values of PC3 (Figure 2g) describe dorsally flattened dactyli with a very dominant, lateral cutting edge, a strong concave arch on the inside and insertion points standing approximately in a 90° angle to the long axis.

Negative values of PC4 (Figure 2h) represent dorsally bent dactyli with a pointed tip, a wavy cutting edge and a concave arch on the dactylus inside. The joint openings are quite similar to the consensus shape. The positive values of PC4 (Figure 2i) include dactyli that are dorsally flattened and exhibit a rounded tip. The lateral located cutting edge is recognizable but not dominant, whereas the joint opening is more dominant than in the consensus shape.

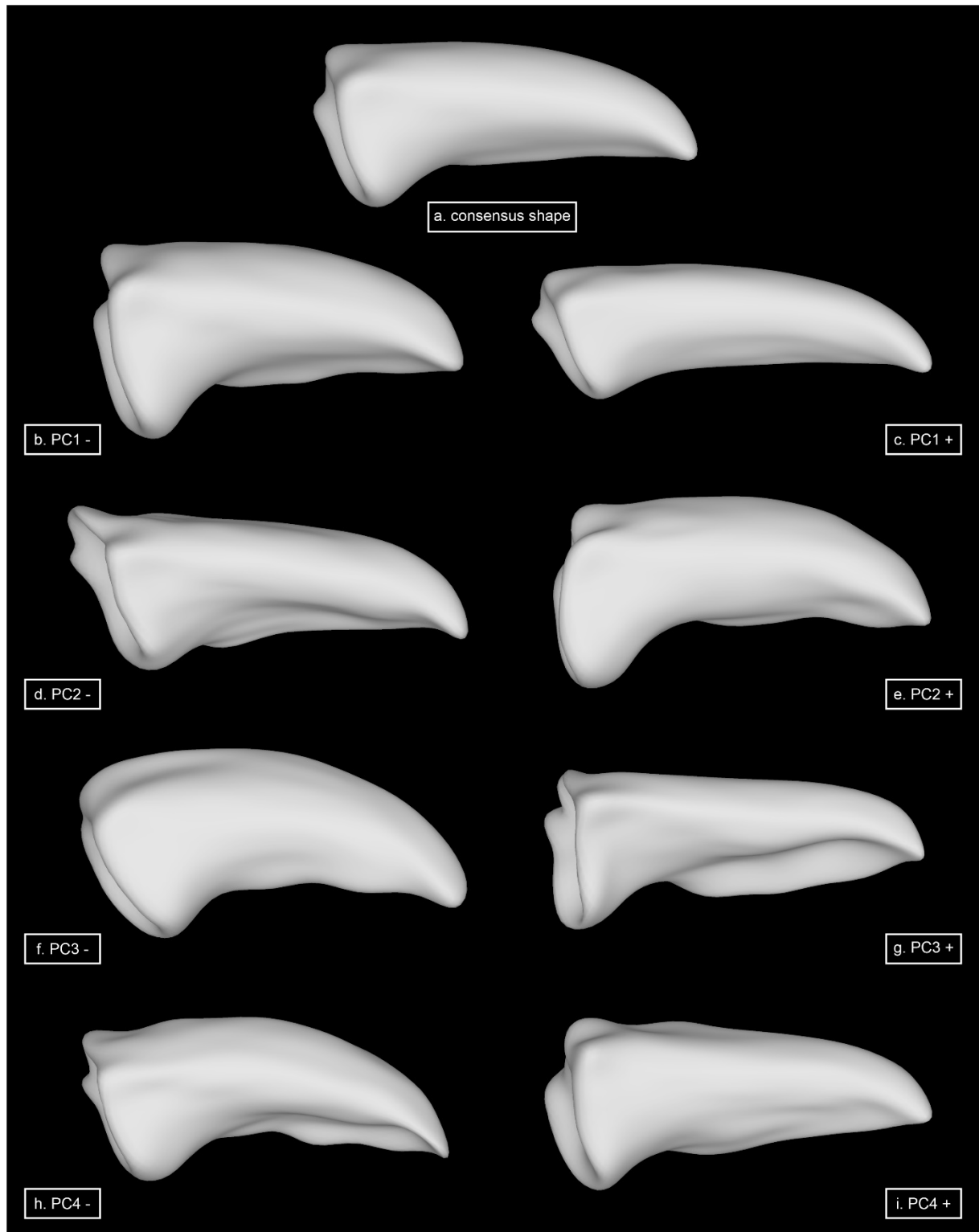


**Figure 2.** Results of the 3D spherical harmonic analyses of dactyli showing major shape variation of the first four principal components compared to the consensus shape (a). All depictions of shape variation comprise exactly the same orientation and proportions.

### **Propodi shape variation**

The first three PCs explain 73.7% of total shape variation (PC1: 38.7%; PC2: 27.4% and PC3: 7.6%).

Negative values of PC1 (Figure 3b) are associated with propodi that exhibit a clinched pollex with a rounded cutting edge. Compared to the consensus shape (Figure 3a), the manus appears more massive, both in length and extent. Insertion points are more dominant compared to the consensus shape. In contrast, positive values of PC1 (Figure 3c) describe a propodus comprising a strongly elongated, dorsally curved pollex and a shortened manus. Insertion points are less dominant compared to the consensus shape.

Negative values of PC2 (Figure 3d) are associated with a less marked, rounded pollex and an elongated manus. The axis of the proximal insertion point is tilted, so that the ventral boundaries of the closure apodems project even further in proximal direction. In contrast, positive values of PC2 (Figure 3e) capture propodi with a dominant spoon-shaped pollex and a distinct cutting edge, whereas the manus is shortened compared to the consensus shape. Also, insertion points are larger and much more distinct, especially the proximal boundaries of the closure apodems.

Negative values of PC3 (Figure 3f) represent propodi with an edged pollex exhibiting a small cutting edge right behind the apex. Compared to the consensus shape, the manus is elongated and along the long axis ventrally flattened. Shape changes associated with positive values of PC3 (Figure 3g) show propodi with an elongated pollex compared to consensus shape. The manus is shortened with insertion points that are both much more dominant, especially the proximal boundaries of the closure apodems (cf. PC2+)

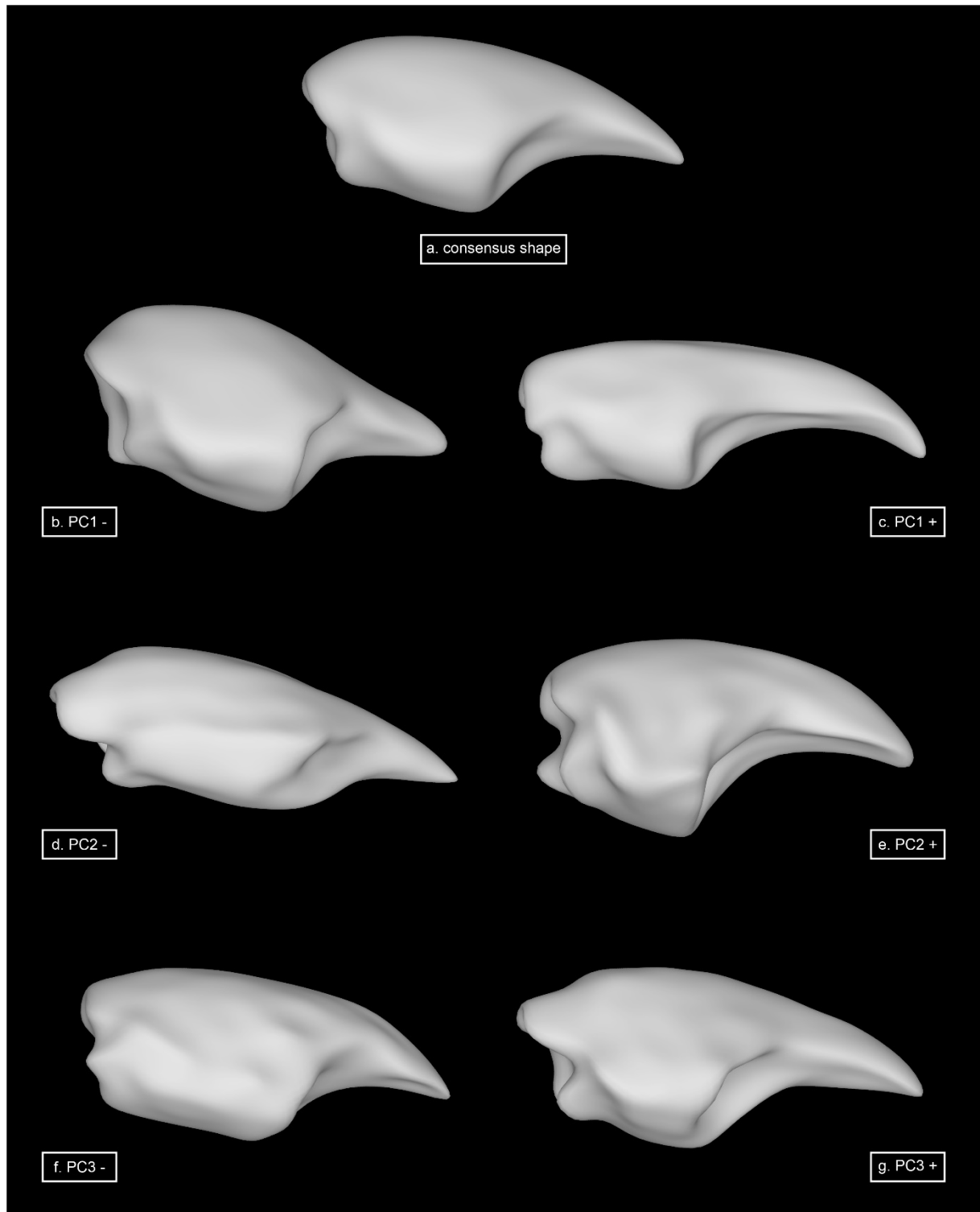


**Figure 3.** Results of the 3D spherical harmonic analyses of propodi showing major shape variation of the first three principal components compared to the consensus shape (a). All depictions of shape variation comprise exactly the same orientation and proportions.

## PCA data output

For the examined dactyli, specimens are mainly distributed into four groups separated along the PC1 and PC2 axes (Figure 4). Right and left dactyli of *C. erythropus* are well separated from other species in an area determined by PC2 values below -0.003. While having a similar extent as *C. erythropus* on the PC1 axis, the group 1 *subdominant diogenid and pagurid claws* separates clearly from other groups by PC2 values above 0.003. Group 4 containing *homoiochelic and dominant diogenid claws* separates from other groups by PC1 values below -0.0015. Dominant claws of *P. cuanensis* represent an extreme in the morphospace with values between 0.009 and 0.01 along the PC1 axis. Dominant claws of *P. anachoretus* are located near the middle of the morphospace and therefore share PC1 value ranges with group 1 and 3 and PC2 value ranges with group 4. In Figure 4a, the morphospace of the PCs 3 and 4 is displayed, wherein only one group, comprised of right and left dactyli of *D. pugilator*, is clearly separated from other specimens by PC3 values below -0.005.

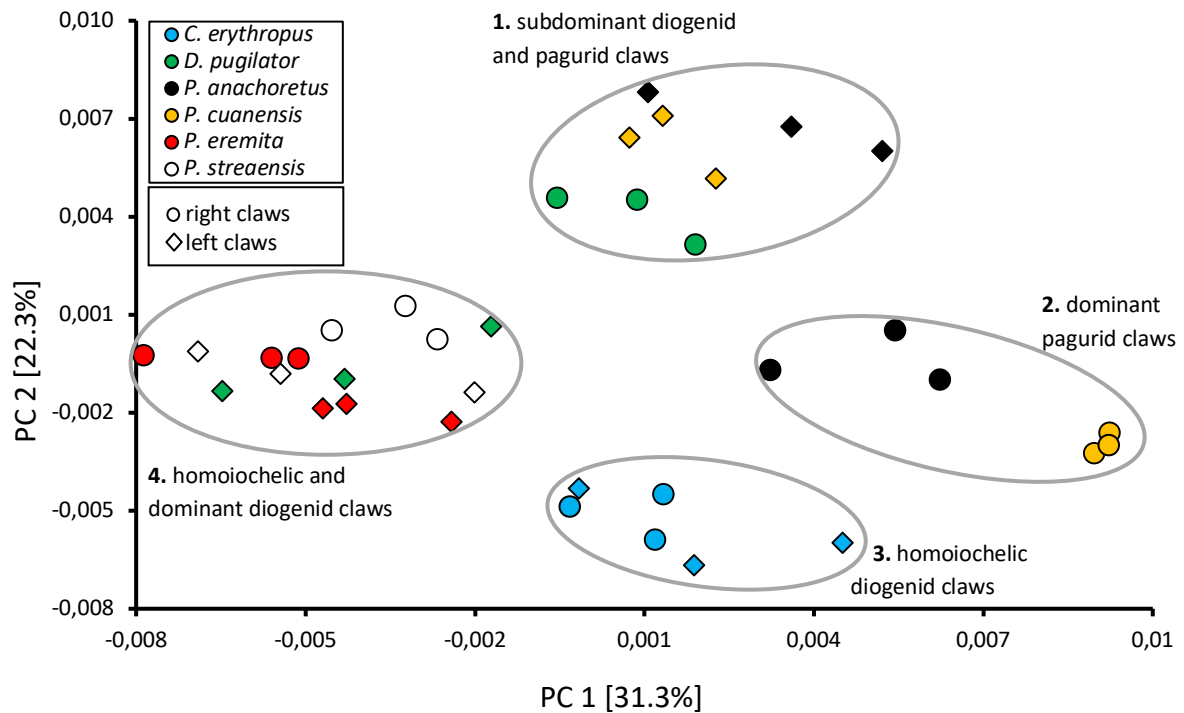


**Figure 4.** Scatterplot of PC1 vs. PC2, whereby every point represents the dactylus of an examined claw. Circles distinguish between groups in the 2D morphospace. The closer points lay together, the more similar the respective dactyli are. In this example, PC1 and PC2 together capture 55.1% of the over-all shape variance and therefore provide a clear first assessment of the data. Group 1: left dactyli of *P. anachoretus*, *P. cuanensis* and right dactyli of *D. pugilator*; group 2: right dactyli of *P. anachoretus* and *P. cuanensis*; group 3: left and right dactyli of *C. erythropus*; group 4: left dactyli of *D. pugilator* and left and right dactyli of *P. eremita* and *P. streaensis*.

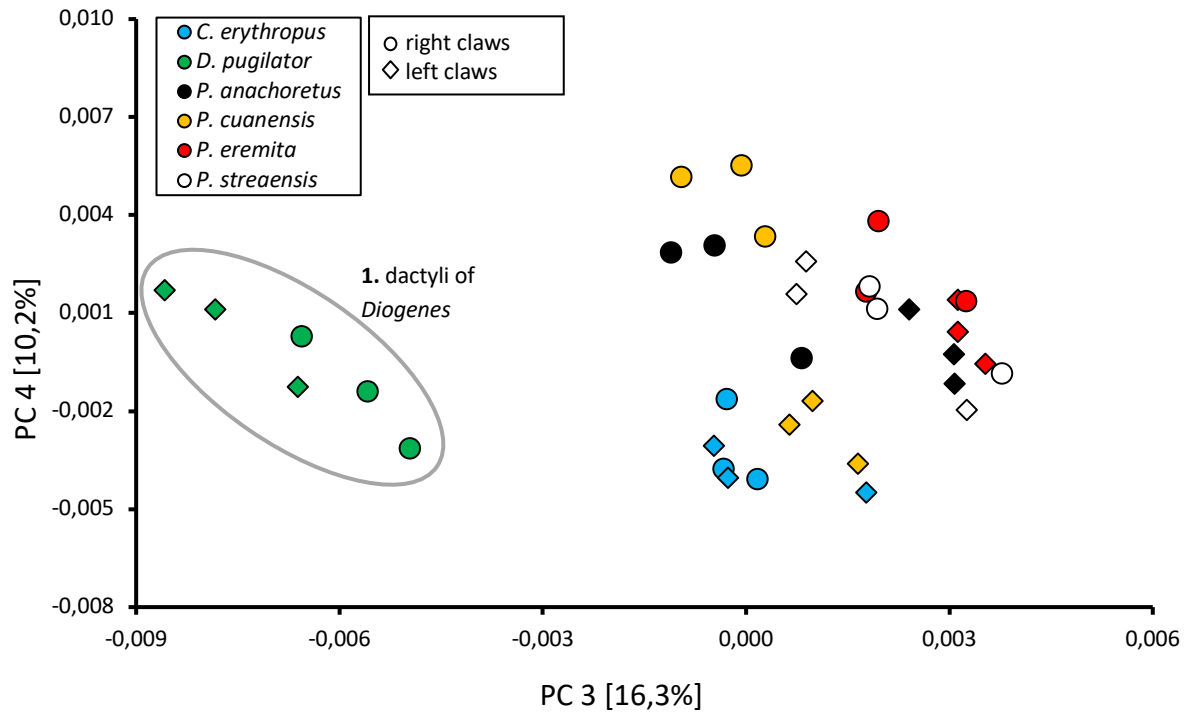


**Figure 4a.** Scatterplot of PC3 vs. PC4, whereby every point represents the dactylus of an examined claw. Circles distinguish between groups in the 2D morphospace. The closer points lay together, the more similar the respective dactyli are. In this plot, PC3 and PC4 together capture 26.5% of the over-all shape variance. Group 1: left and right dactyli of *D. pugilator*.

In the morphospace for propodi (Figure 5), *dominant claws of D. pugilator* (group 1) clearly demarcate from other claws along the PC1 and PC2 axes with PC values around -0.008. Group 2 containing *dominant claws of Paguristes* is also clearly separated in the morphospace likewise group 3, composed of *Clibanarius* and *subdominant claws of Paguristes*. *Subdominant pagurid claws* (group 4) comprise the highest values along the PC1 axis and therefore separate from other claws in the morphospace. In the scatter plot for propodi comprising of PCs 1 and 3 (Figure 5a), the groupings are less distinct. But the groups one, two and four (cf. Figure 5) are still recognizable.



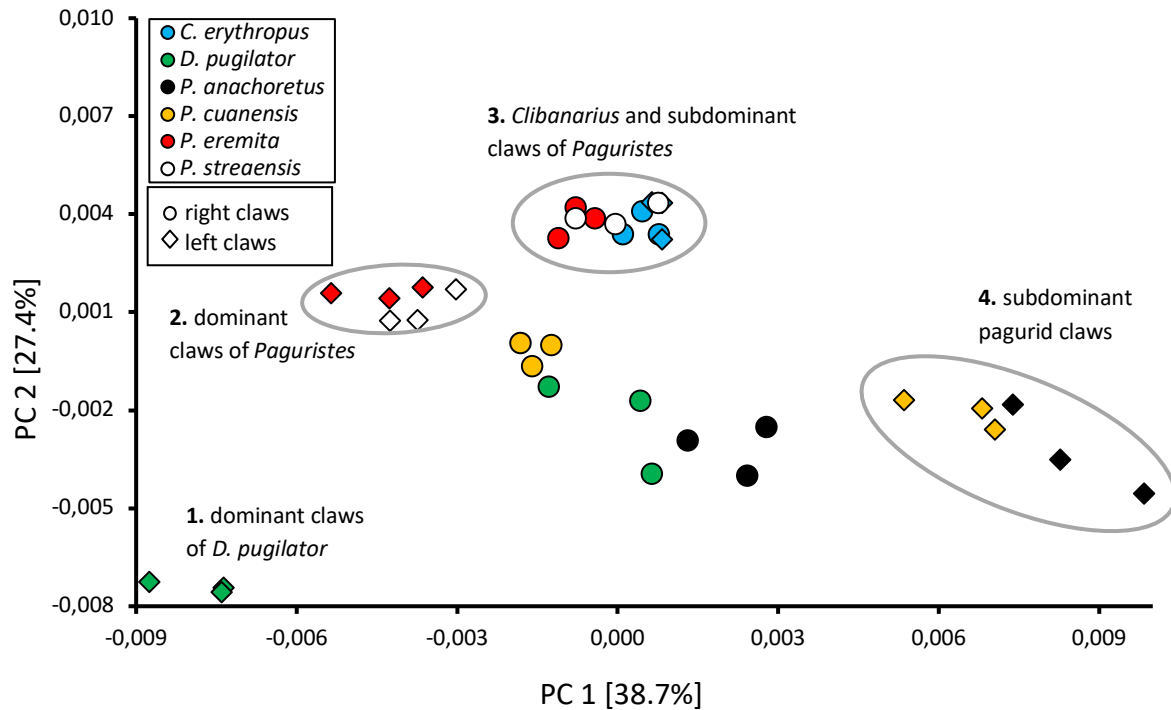


**Figure 5.** Scatterplot of PC1 vs. PC2, whereby every point represents the propodus of an examined claw. Circles distinguish between groups in the 2D morphospace. The closer points lay together, the more similar the respective propodi are. In this example, PC1 and PC2 together capture 65.1% of the over-all shape variance. Group 1: left propodi of *D. pugilator*; Group 2: left propodi of *P. streaensis* and *P. eremita*; Group 3: right propodi of *P. streaensis*, *P. eremita* and both propodi of *Clibanarius*; Group 4: left propodi of *P. anachoretus* and *P. cuanensis*.

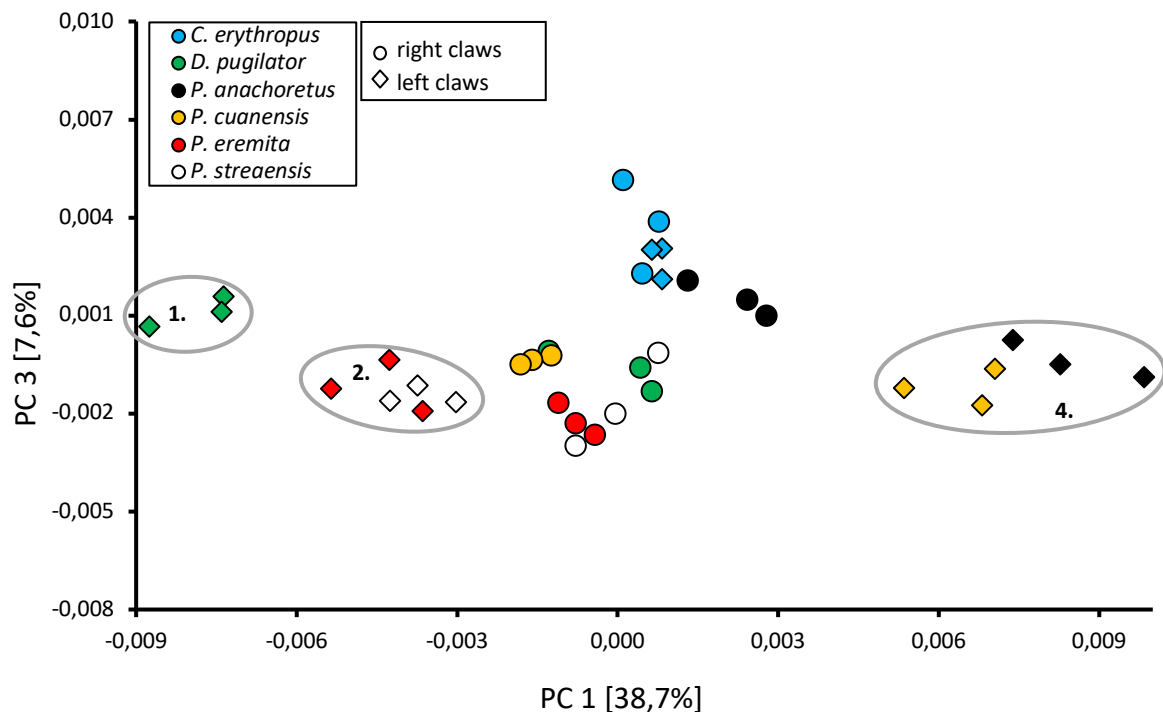


**Figure 5a.** Scatterplot of PC1 vs. PC3, whereby every point represents the propodus of an examined claw. The closer points lay together, the more similar the respective propodi are. In this example, PC1 and PC3 together capture 46.3% of the over-all shape variance. Group 1: left propodi of *D. pugilator*; Group 2: left propodi of *P. streaensis* and *P. eremita*; Group 4: left propodi of *P. anachoretus* and *P. cuanensis*.

## Multivariate statistics

For dactyli, the separation between Diogenidae and Paguridae was highly significant ( $p < 0.0001$  for MANOVA and npMANOVA) whereby a separation between right and left dactyli across families did not show any significant relation ( $p > 0.05$ ). Concerning the CVA, results show significant separations between all groups except left and right diogenid claws, which overlap in Figure 6 (see Table 2).

**Table 2.** Results of the MANOVA (top) and npMANOVA (bottom) of the groupings Diogenidae left, Diogenidae right, Paguridae left and Paguridae right. F-values are colorized green, p-values orange and the root of Mahalanobis distances (MD) blue.

|                  |                 |                  |                |                 |
|------------------|-----------------|------------------|----------------|-----------------|
| F-value = 16.9   | Diogenidae left | Diogenidae right | Paguridae left | Paguridae right |
| Diogenidae left  | p-value         | 0.6380           | <0.0001        | <0.0001         |
| Diogenidae right | 1.7076          |                  | 0.0003         | <0.0001         |
| Paguridae left   | 34.6541         | 21.1358          |                | 0.0044          |
| Paguridae right  | 38.2350         | 32.3538          | 36.3067        | root (MD)       |

|                  |                 |                  |                |                 |
|------------------|-----------------|------------------|----------------|-----------------|
|                  | Diogenidae left | Diogenidae right | Paguridae left | Paguridae right |
| Diogenidae left  | p-value         | 1.0              | 0.0012         | 0.0012          |
| Diogenidae right | 0.8962          |                  | 0.0006         | 0.0006          |
| Paguridae left   | 15.1800         | 10.3100          |                | 0.0114          |
| Paguridae right  | 13.7            | 13.3100          | 30.71          | F-value         |

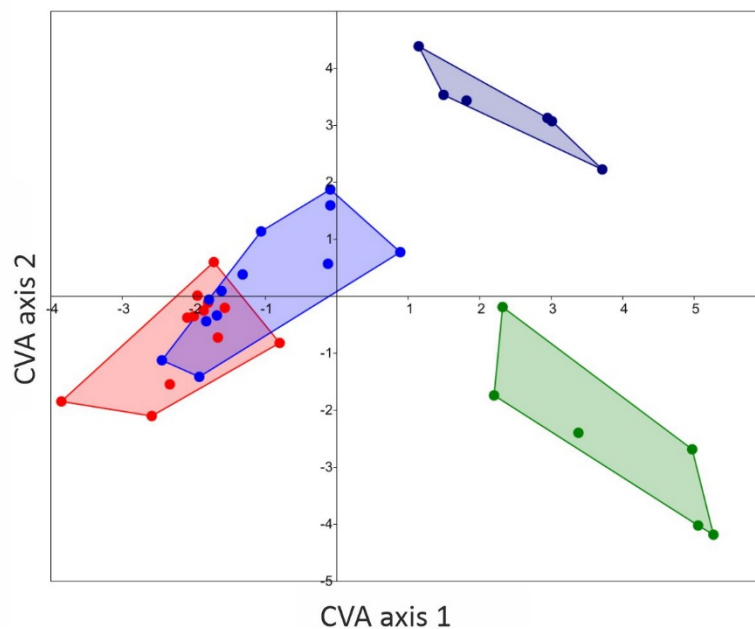


**Figure 6.** CVA scatter plot of the groupings diogenid left dactyli (red), diogenid right dactyli (blue), pagurid left dactyli (dark blue) and pagurid right dactyli (green).

For the propodi, the separation of Diogenidae and Paguridae was highly significant ( $p < 0.0001$  for MANOVA and  $p = 0.0001$  npMANOVA) whereby a separation of all examined right and all examined left propodi did not show significant relations ( $p > 0.05$ ). The results of the CVA only show a significant separation between the pagurid left propodi. The remaining groupings overlap at least with one other group (see Figure 7, Table 3).

**Table 3.** Results of the MANOVA (top) and npMANOVA (bottom) of the groupings Diogenidae left, Diogenidae right, Paguridae left and Paguridae right. F-values are colored green, p-values orange and the root of Mahalanobis distances (MD) blue.

|                        |                        |                         |                       |                        |
|------------------------|------------------------|-------------------------|-----------------------|------------------------|
| <b>F-value = 12.68</b> | <b>Diogenidae left</b> | <b>Diogenidae right</b> | <b>Paguridae left</b> | <b>Paguridae right</b> |
| Diogenidae left        | p-value                | 0.0169                  | <0.0001               | 0.0140                 |
| Diogenidae right       | 3,6247                 |                         | <0.0001               | 0.4395                 |
| Paguridae left         | 51.8993                | 31.9707                 |                       | 0.0046                 |
| Paguridae right        | 6.8904                 | 2.4708                  | 21.3673               | root (MD)              |

|              |                     |                     |                    |                    |
|--------------|---------------------|---------------------|--------------------|--------------------|
|              | <b>Diogenidae L</b> | <b>Diogenidae R</b> | <b>Paguridae L</b> | <b>Paguridae R</b> |
| Diogenidae L | p-value             | 0.0876              | 0.0006             | 0.2988             |
| Diogenidae R | 4.8440              |                     | 0.0018             | 0.0750             |
| Paguridae L  | 21.3500             | 26.9200             |                    | 0.0114             |
| Paguridae R  | 2.9000              | 5.0570              | 25.6000            | F-value            |

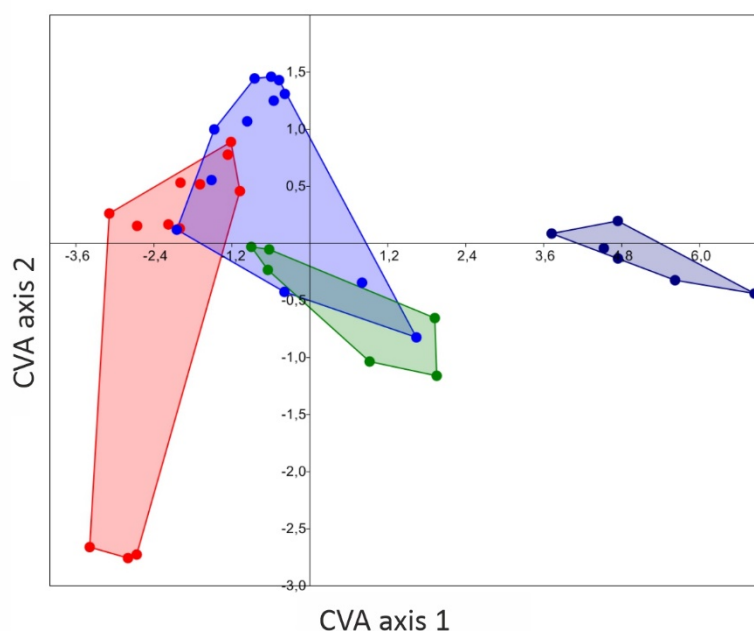


**Figure 7.** CVA scatter plot of the groupings diogenid left propodi (red), diogenid right propodi (blue), pagurid left propodi (dark blue) and pagurid right propodi (green).

## Discussion

The final transformation of harmonized 3D meshes via PCs allows the quantification of shape variation that can be further processed with different multivariate analyses, including MANOVA, CVA and disparity analyses, afterwards. By illustrating numeric values of the first two PCs as a scatter plot for dactyli (Figure 4), on the one hand, one can easily discriminate between dominant and subdominant claws of heterochelic species, e.g. *P. anachoretus*, *D. pugilator* and even illustrate different levels of intraspecific variability regarding dominant and subdominant claws, e.g. *P. cuanensis*. On the other hand, claws of homiochelic species such as *C. erythropus* or *P. eremita* and *P. streaensis* cluster together. Concerning the propodi (Figure 5), the discrimination of dominant and subdominant claws also is easy to recognize, whereas homiochelic claws cluster together (cf. *C. erythropus*). Of all examined hermit crab claws, dominant propodi of *D. pugilator* have the least divergence and are clearly separated from other species in the morphospace (Figure 5). We consider the present study as a case study for the introduction of our newly established methodology, showing that it is well suited for detailed shape investigations. Future studies with larger sample size will show whether claw shape is more determined by a phylogenetic signal with higher similarities in claw shape between species within the same family than between species ranking in different families or by a stronger functional signal with stronger shape resemblance in dominant (right claw in Paguridae and Lithodoidea, left claw in Diogenidae and Coenobitidae) and subdominant claws beyond family boundaries.

## Summary

A procedure is described making SPHARM-based GM approachable for 3D segmentations that contain large cavity openings. In this case study, we examined 3D shape of the dactyli and propodi of hermit crab claws whereby insertion points were closed using an algorithm based on AO before surfaces were calculated and employed to shape analyses. Finding the most optimal geometrical solution for the closure, AO can be reproduced more objectively than hand-made closures, extending the application range of SPHARM to biological structures that are more complex in their morphology. Applying the described methods to our data lead to results which are precise and suitable to study the inter- and intraspecific differences in shape of hermit crab claws and are highly suitable for further statistical analyses as PCA, MANOVA and CVA. Furthermore, the procedure is easy to reproduce and creates sparse variance in the data, closures integrate smoothly into the total structures and the algorithm saves significant amounts of time.

## Acknowledgments

Sincere thanks are given to Stephan Scholz for the technical support. Many thanks to the team of MareMundi for assisting with sampling.

## Compliance with ethical standards

**Conflict of interest** All authors declare that they have no conflict of interest.

**Ethical approval** All applicable international, national, and institutional guidelines for the care and use of animals were followed. No endangered species or animals from protected areas were used for this study. This article does not contain any studies with human participants performed by any of the authors.

## References

- Adams, D.C., Rohlf, F.J. & Slice, D.E. (2004): Geometric morphometrics: Ten years of progress following the 'revolution'. *Italian Journal of Zoology* 71, 5-16.
- Baum, D. & Titschack, J. (2016): Cavity and pore segmentation in 3D images with ambient occlusion. In: Bertini, E., Elmqvist, N., Wischgoll, T. (eds.), *Eurographics Conference on Visualization (EuroVis)*. Pp. 113-117. The Eurographics Association.
- Bookstein, F.L. (1991): Landmarks. In: *Morphometric Tools for Landmark Data: Geometry and Biology*. Cambridge University Press, New York, 55-87.
- Bookstein F.L. (1997): Landmark methods for forms without landmarks: morphometrics of group difference in outline shape. *Medical Image Analysis* 1, 225-243.
- Brechtbühler, C., Gerig, G. & Kübler O. (1995): Parametrization of closed surfaces for 3-D shape description. *Computer Vision and Image Understanding* 61, 154-170.
- Curtis, A.A. & van Valenburgh, B. (2014): Beyond the sniffer: Frontal sinuses in carnivora. *The Anatomical Record* 297, 2047-2064.
- Cignoni, P., Callieri, M., Corsini, M., Dellepiane, M., Ganovelli, F. & Ranzuglia, G. (2008): MeshLab: an open-source mesh processing tool. *Eurographics Italian Chapter Conference* 6, 129-136.
- Elewa, A.M.T. (2004): *Morphometrics - Applications in biology and paleontology*. Springer Verlag, pp. 55-65.
- Felice, R.N. & Goswami, A. (2017): Developmental origins of mosaic evolution in the avian cranium. *Proceedings of the National Academy of Sciences of the United States of America* 115, 555-560.
- Foth, C., Evers, S.W., Joyce, W.G., Volpato, V.S. & Benson, R.B.J. (2019): Comparative analysis of the shape and size of the middle ear cavity of turtles reveals no correlation with habitat ecology. *Journal of Anatomy*. Published online. doi: 10.1111/joa.13071
- Gower, J.C. (1975): Generalized procrustes analysis. *Psychometrika* 40, 33-51.
- Gunz, P., Mitteroecker, P. & Bookstein, F.L. (2005): Semilandmarks in three dimensions. In: Slice D.E. (eds.), *Modern Morphometrics in Physical Anthropology. Developments in Primatology: Progress and Prospects*. Springer, Boston, Pp. 73-98.
- Hammer, Ø., Harper, D.A.T. & Ryan, P.D. (2001): PAST: Paleontological statistics software package for education and data analysis. *Palaeontologia Electronica* 4, 1-9.
- Hammer, Ø. & Harper, D.A.T. (2006): *Paleontological data analysis*. Pp. 351. Malden: Blackwell Publishing Ltd.
- Jackson, D.A. (1993): Stopping rules in principal components analysis: A comparison of heuristical and statistical approaches. *Ecology* 74, 2204-2214.

- Manfreda, E., Mitteroecker, P., Bookstein, F.L. & Schaefer, K. (2006): Functional morphology of the first cervical vertebra in humans and nonhuman primates. *Anatomical Record Part B: New Anatomist* 289, 184–194.
- McPeck, M.A., Shen, L. & Farid, H. (2009): The correlated evolution of three-dimensional reproductive structures between male and female damselflies. *Evolution* 63, 73-83.
- McPeck, M.A., Symes, L.B., Zong, D.M. & McPeck, C.L. (2011): Species recognition and patterns of population variation in the reproductive structures of a damselfly genus. *Evolution* 65, 419-428.
- Mitteroecker, P. & Freudenthaler, J.W. (2012): Geometrische Morphometrie – ein Paradigmenwechsel in der Kieferorthopädie steht an. *Informationen aus Orthodontie und Kieferorthopädie* 44, 17-22.
- Mitteroecker, P. & Gunz, P. (2009): Advances in Geometric Morphometrics. *Evolutionary Biology* 36, 235-247.
- Pearson, K. (1901): On lines and planes of closest fit to a system of points in space. *The London, Edinburgh, and Dublin Philosophical Magazine and Journal of Science* 6, 559–572.
- Pomidor, B.J., Makedonska, J. & Slice, D.E. (2016): A landmark-free method for three-dimensional shape analysis. *Plos One* 11, 3.
- Rohlf, F.J. & Marcus, L.F. (1993): A revolution in morphometrics. *Trends in Ecology & Evolution* 8, 129-132.
- Schäfer, W. (1954): Form und Funktion der Brachyuren-Schere. *Abhandlung der Senckenbergischen naturforschenden Gesellschaft* 489. Senckenberg am Meer Nr. 164. Pp. 65. Frankfurt a. Main: W. Kramer & Co.
- Shen, L., Farid, H. & McPeck, M.A. (2009): Modeling three-dimensional morphological structures using spherical harmonics. *Evolution* 63, 1003-1016.
- Shen, L. & Makedon, F. (2006): Spherical mapping for processing of 3D closed surfaces. *Image and Vision Computing* 24, 743-761.
- Zelditch, M.L., Swiderski, D.L., Sheets, H.D. & Fink, W.L. (2004): Geometric Morphometrics for Biologists: A Primer. Pp. 443. Elsevier Academic Press, San Diego.